IET Renewable Power Generation

Research Article

IET Journals
The Institution of Engineering and Technology

Linear generator-based wave energy converter model with experimental verification and three loading strategies

ISSN 1752-1416
Received on 20th March 2015
Revised on 20th July 2015
Accepted on 8th September 2015
doi: 10.1049/iet-rpg.2015.0117
www.ietdl.org

Yue Hong[1] ✉, *Mikael Eriksson*[2], *Valeria Castellucci*[1], *Cecilia Boström*[1], *Rafael Waters*[1,2]

[1]*Division for Electricity, Uppsala University, SE-751 21 Uppsala, Sweden*
[2]*Department of Engineering Sciences, Seabased AB, SE-751 21 Uppsala, Sweden*
✉ *E-mail: yue.hong@angstrom.uu.se*

Abstract: Within the Lysekil wave energy research project at the Swedish west coast, more than ten Wave Energy Converters (WECs) prototypes have been developed and installed in an ocean based test site. Since 2006 various experiments have been conducted and the generated electricity was delivered to shore at a nearby island. While experiments are essential for the development of wave energy converters, theoretical studies and simulations are an important complement – not only in the search for advanced designs with higher efficiency, but also for improving the economic viability of the studied concepts. In this paper a WEC model is presented. The model consists of three subsystems: i) the hydrodynamic source, ii) the linear generator model, and iii) the electrical conversion system. After the validation with the experimental results at the research site, the generator model is connected to three passive load strategies – linear resistive load, passive rectification and resonance circuit. The paper focuses on analysing the operation of the model coupled with three load cases. The results prove that the WEC model correctly simulates the linear generator developed in the Lysekil Project. Moreover, the comparison among different load cases is made and discussed. The results gives an indication of the efficiency of energy production as well as the force ripples and resulting mechanical loads on the wave energy converters.

1 Introduction

The direct drive linear generator developed in the Lysekil Project consists of one movable part and stationary part. The movable part, the so-called translator, is covered with rows of permanent magnets, whereas the stationary part, called stator, is winded with conductive cables. The structure of the linear generator is illustrated in Fig. 1*a*.

The generator is standing on the seabed and it is connected to a floating buoy which moves mostly in heave motion, inducing a vertical motion of the translator inside the stator [1]. When the wave comes, the buoy is driven and thus pulling the translator to move with the wave motion. In the meantime, the magnets on the translator move in relation to the stator winding, instantaneously inducing a three-phase voltage inside the stator winding. As the linear generator is connected to the load, instantaneous electrical power is produced and transmitted out from the generator to the load [2].

In 2013, a new marine substation is deployed and connected to two linear generators, as shown in Fig. 1*b*. The electric system inside the substation includes the insulated gate bipolar transistor bridge and the DC/DC converter for rectification and electrical control. In the Lysekil Project so far, three different control strategies [3] have been experimentally tested. They are the passive diode rectification, DC/DC control, and resonance circuit [4].

In this paper, a simulated generator model was built. The specification of the generator called *L9* in the Lysekil Project was utilised as the reference for the model. After the introduction, Section 2 presents the validation of the generator model. A comparison was carried out between the simulated and experimental results. In Section 3, the model was coupled to the hydraulic wave system. In the hydraulic model, the hydrodynamic function was built to emulate the motion of the buoy body when it reacted to the sea wave. The hydraulic model supplied a continuous excitation to drive the translator's vertical motion. Different load cases were also studied when the generator model was connected to the electrical system. Results and discussion are presented in Section 4.

Comparing with other's work which has already been published within the same research group [5], the novelties of this paper is the validation of the generator model with the *L9* specifications. In addition, the analysation on the model with the resonant circuit case has not yet been done before. Future studies will include correlations among damping force, generated power, and phase current. In addition to the studied load strategies, active control of various types will be included – the goal being to optimise energy absorption and total system efficiency.

2 Verification of linear generator model

2.1 Linear generator model

In the linear generator, the magnetic flux is generated by the permanent magnets on the translator. The flux is confined inside the magnetic path along the laminated steel sheets, isolated conductors mounted on the stator, air gaps etc [6]. Assuming that the magnetic flux has sinusoidal form, the flux can be described as

$$\phi = \phi_0 \sin(kx + \theta) \tag{1}$$

In the equation above, k is the wave number which $k = 2\pi/\lambda$, λ is the wavelength. ϕ_0 is the magnitude of the magnetic flux, x is the distance of the translator, and θ is the phase shift.

If the magnetic flux is time dependent on the x-axis, the flux can be derived with respect to time

$$\frac{\mathrm{d}\phi}{\mathrm{d}t} = k\phi_0 \cos(kx + \theta) \cdot \frac{\mathrm{d}x}{\mathrm{d}t} \tag{2}$$

According to Faraday's Law, when the magnetic flux is induced and

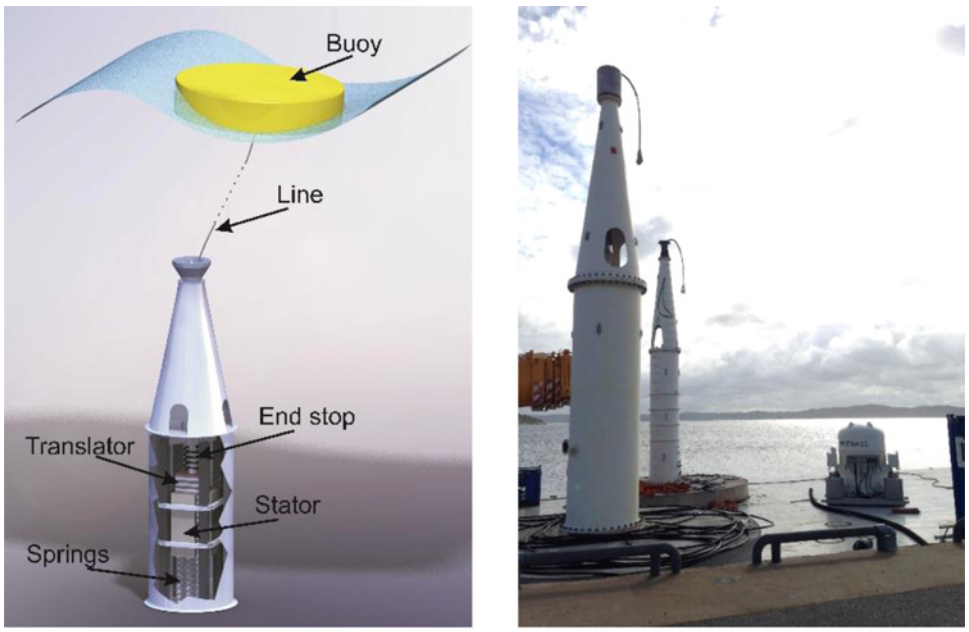

Fig. 1 *Generators in the Lysekil Project*

a Illustration of the *L*1 generator
b Generators *L*6 and *L*9 waiting to be launched and the marine substation

flows through the path of magnet circuit, the voltage is also generated according to the change of magnetic flux over time. The induced open-circuit voltage is expressed as

$$\varepsilon = -N\frac{\mathrm{d}\phi}{\mathrm{d}t} \tag{3}$$

where N is the number of turns of the winding inside the stator.

Inserting (2) into the right-hand side of (3), then (4) is obtained

$$\varepsilon = -Nk\phi_0 \cos(kx+\theta)\cdot\frac{\mathrm{d}x}{\mathrm{d}t} \tag{4}$$

The equation above represents the core of the energy conversion theory and it shows the mechanical performance of the linear generator. For the three-phase generator, like *L*9, the induced three-phase voltage is described by the system of (5)

$$\begin{cases} \varepsilon_a = -Nk\phi_0 \cos(kx)\cdot\dfrac{\mathrm{d}x}{\mathrm{d}t} \\ \varepsilon_b = -Nk\phi_0 \cos\left(kx+\dfrac{2\pi}{3}\right)\cdot\dfrac{\mathrm{d}x}{\mathrm{d}t} \\ \varepsilon_c = -Nk\phi_0 \cos\left(kx-\dfrac{2\pi}{3}\right)\cdot\dfrac{\mathrm{d}x}{\mathrm{d}t} \end{cases} \tag{5}$$

In this paper, the parameters of a wave energy converter (WEC) prototype, the *L*9, are utilised to verify the linear generator model, in particular, its output power as well as its performance.

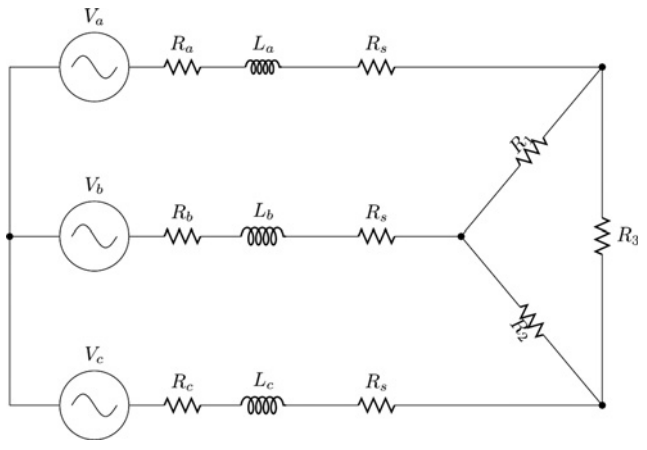

Fig. 2 *Circuit diagram of the generator connected with three-phase resistive load*

2.2 Calculation of A factor

In the generator, the output voltage is also influenced by the active area between the stator and translator. The area represents the coverage of the magnetic circuit, contributing to the electrical energy production. However, the length of the translator is finite. As one end of the translator is slipping out from the stator, the active area decreases. As a result, the output three-phase voltage is not fully induced. To describe how much surface of the stator is active, the A factor [7] is used. The A factor is independent from the speed of wave, wave frequency, and height of the wave, but directly depending on the position of the translator's central point instead. It is included into the voltage calculation, and regarded as an indispensable factor when building the linear generator model. The system of (6) shows how the A factor varies with respect to the position of the translator's central point x

$$A(x)_{\mathrm{fac}} = \begin{cases} 1, & |x| < \alpha \\ \dfrac{1}{\alpha-\beta}(|x|-\alpha)+1, & \alpha < |x| < \beta \\ 0, & |x| > \beta \end{cases} \tag{6}$$

According to Kirchhoff's Law, the voltages have to fulfil the system

IET Renew. Power Gener., 2016, Vol. 10, Iss. 3, pp. 349–359

Table 1 *L9* specifications

L9 specifications	
nominal power at 0.7 m/s	20 kW
voltage, line-to-line, root mean square at 0.7 m/s	450 V
generator resistance	1 ± 1.5% Ω
generator inductance	20 mH
air gap	3 mm
pole width	55 mm
vertical stator length	2000 mm
vertical translator length	2000 mm
translator weight	2700 kg

Table 2 Parameters for the resistive load

Parameters for the resistive load	
resistance on each phase experiment	15 Ω
resistance on each phase adjust	15.9 Ω
sea cable resistance	0.54 ± 1.5% Ω
sea cable inductance	<0.01 mH
sea cable capacitance	145 μF

of (7)

$$\begin{cases} \varepsilon_a A(x)_{\text{fac}} = Ri_a + L\dfrac{\mathrm{d}i_a}{\mathrm{d}t} + U_a \\ \varepsilon_b A(x)_{\text{fac}} = Ri_b + L\dfrac{\mathrm{d}i_b}{\mathrm{d}t} + U_b \\ \varepsilon_c A(x)_{\text{fac}} = Ri_c + L\dfrac{\mathrm{d}i_c}{\mathrm{d}t} + U_c \end{cases} \tag{7}$$

Taking the linear generator *L9* as an example, the factors α and β are $\alpha = 0$, $\beta = 2$ respectively, then the A factor can be calculated as

$$A(x)_{\text{fac}} = \begin{cases} 0, & |x| > 2 \\ 1 - \dfrac{1}{2}|x|, & 0 < |x| < 2 \end{cases} \tag{8}$$

2.3 Load connected to the generator

As the preliminary step to validate the generator model, the three-phase resistive load is applied to the output ports of the

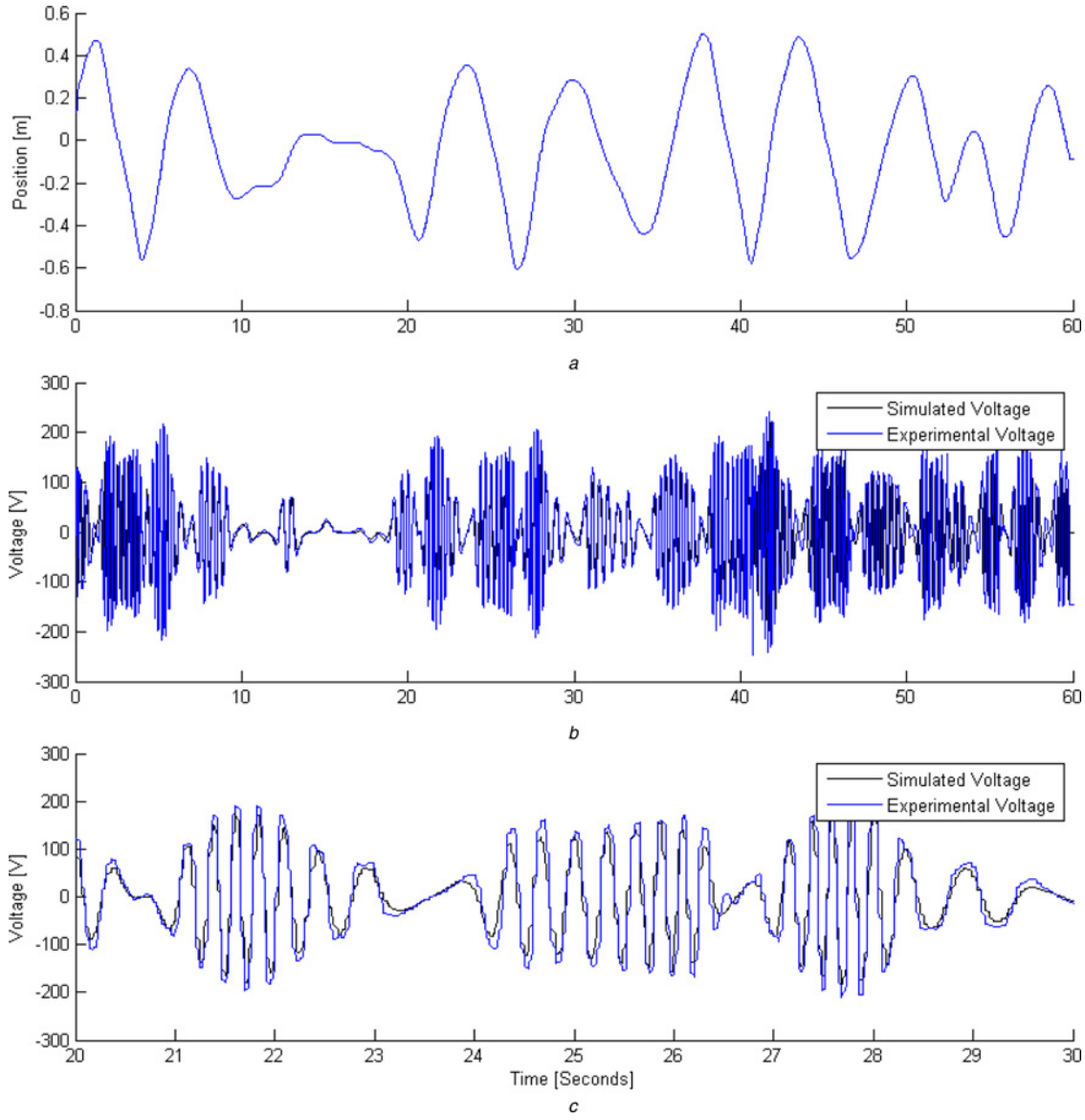

Fig. 3 *Output phase voltage from the linear generator model according to the movement of the translator*

a Position of the translator's middle point
b Comparison between experimental and simulated phase voltages output from the linear generator
c Comparison between experimental and simulated phase voltages within 10 s

model. The test gives a direct view on the performance of the generator when the buoy is having the vertical motion which is driven by the waves. In Fig. 2, the resistive load is designed as delta connection, and is connected to the sea cable on the generator's output side [8].

2.4 Verification of the generator model

In this simulation case, the specification of *L*9 is taken as the reference to build the linear generator model. Accordingly, the experimental results from the measurement are utilised to validate the performance of the generator model. The specifications are shown in Table 1.

The generator model is directly connected to the three-phase resistive load, with the parameters used in Table 2. The results are shown in Fig. 3, including (a) the position of the translator [9] and (b) the comparison between the experimental and the simulated phase voltages. Fig. 3*a* shows the movement of the translator's middle point. It is vital for calculating the A factor, which influences the power production. Fig. 3*b* gives a clear graphical view on the comparison between the experimental and the simulated phase voltages within the testing period of 60 s, and (c) is the comparison within 10 s. The result shows that the simulation matches with the experiment quite well. The differences between the experimental and the simulated curves are mainly due to the data loss in the measuring system, causing imprecise performance of the generator model. For example, it is supposed to be a spike of voltage on 42 s in Fig. 3*b* according to the experimental result. Actually the spike in the simulated result is not high enough, possibly due to data loss on the velocity of the translator (Fig. 3*a*). Additionally, the measuring frequency during measurement could as well lead to inaccuracy for experimental validation.

3 Model study of different load cases

3.1 Harmonic excitation and no-load test

A no-load test is first performed on the generator model together with the hydrodynamic model aiming to analyse the performance of the generator. In the no-load test, the translator is driven by the harmonic wave – causing a reciprocating motion. We have chosen a harmonic wave because the studied loads are non-linear and we have aimed for fast simulations in time domain that can provide us with a qualitative way of understanding the effect of the loading

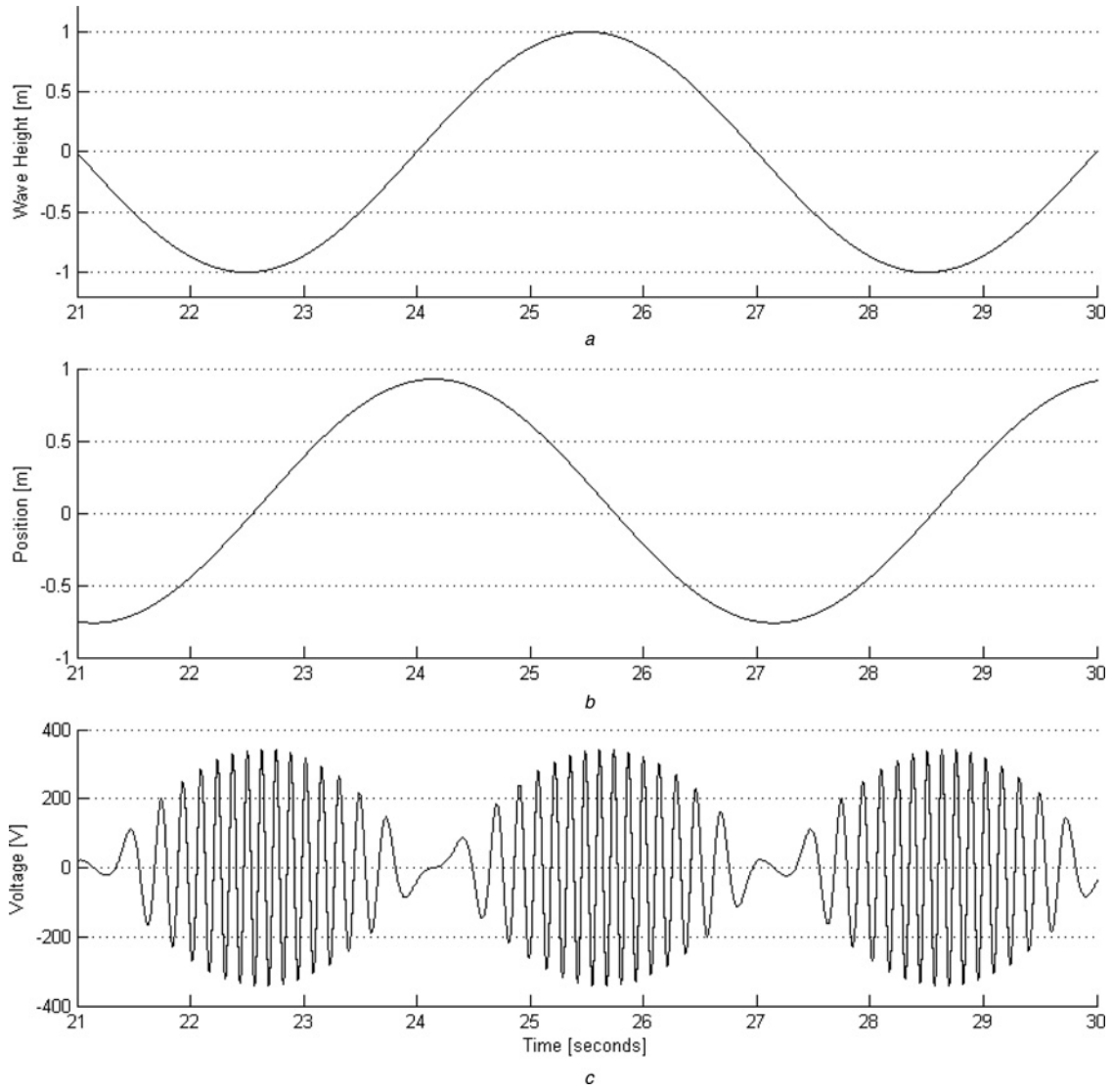

Fig. 4 *Simulated outputs from the generator model coupled with the hydraulic wave source*

a Wave height of the harmonic wave
b Position of the translator's central point
c One phase voltage output from the linear generator

IET Renew. Power Gener., 2016, Vol. 10, Iss. 3, pp. 349–359

strategies on the operation, energy, and forces in the WECs, and to compare the strategies to one another.

The harmonic excitation is generated from the numerical model of the hydrodynamic function. The hydrodynamic model was built by Mikael Eriksson. It emulates the interaction between the buoy and the waves, and thus introducing an excitation force for driving the translator to move. The theory of the model can be referred to [10, 11].

The wave height and the wave period during the study were 2 m and 6 s, respectively, see Fig. 4*a*. As seen in [8], these values are close to the realistic wave conditions at the Lysekil wave energy research site.

Fig. 4*b* shows the harmonic movement of the translator's middle point, with a 90° phase lagging behind the wave motion. Additionally, the average position of the translator's middle point is shifted due to the buoy function and the gravity of the translator. A three-phase no-load voltage is induced inside the generator model and one of these phases is illustrated in Fig. 4*c*. The waveform shows the correlation between the velocity of the translator and the electrical frequency of the output voltage. As expected, the induced voltage and the frequency both decrease as the speed of the translator decreases.

3.2 Harmonic excitation and three load strategies

3.2.1 Linear load: The linear load is a resistive load, as mentioned in Section 2. The parameters for the study are presented in Table 2. The resistance marked with 'experiment' is the parameter used in the experiment, while the resistance marked with 'adjust' means the adjusted values to be used in the simulation, which are chosen in order to gain the same energy output with other load cases. The resulting current and voltage are both shown in Fig. 5. Since an idealised condition is considered (purely resistive load), no reactive power is transferred to the load, meaning that the power factor is equal to 1. For the three-phase resistive load, the load voltage is supposed to be the same as the output voltage of the generator, if the resistance of the sea cable is neglected. In this case, the capacitance of the sea cable is neglected because the actual cable used in the experiments is over-dimensioned; the capacitance is only 145 μF. The negligible impact of this capacitance is the reason why the model connected to the linear load has a unity power factor.

3.2.2 Passive rectification and filter: In the Lysekil research site, off the Swedish West coast, a three-phase diode-bridge was used as a full-wave rectifier, converting the AC voltage generated from the *L*9 generator into a DC voltage, the circuit diagram is shown in Fig. 6. A π-section filter is applied at the DC side [12]. This circuit is built up and connected to the linear generator model in the simulation to observe the response. The parameters of the experiment are presented in Table 3, and are also utilised for the circuit inside the simulation. In this table, the resistance value marked with experimental (EXP) is applied in the experiment, whereas the adjusted (ADJ) means the adjusted value to be used for the simulation, with the same reason as the adjusted value for the pure resistive load.

Fig. 7 describes the simulated output from the generator model. The output AC current from the generator terminals is shown, as well as the rectified voltage and load current after the π-section filter. In Fig. 7*a*, there is no output current when the voltage over the diode is lower than the diode's onset voltage, which explains the shape of the current output. The capacitor bank at the load side succeeds to increase the peak current, due to the discharging effect

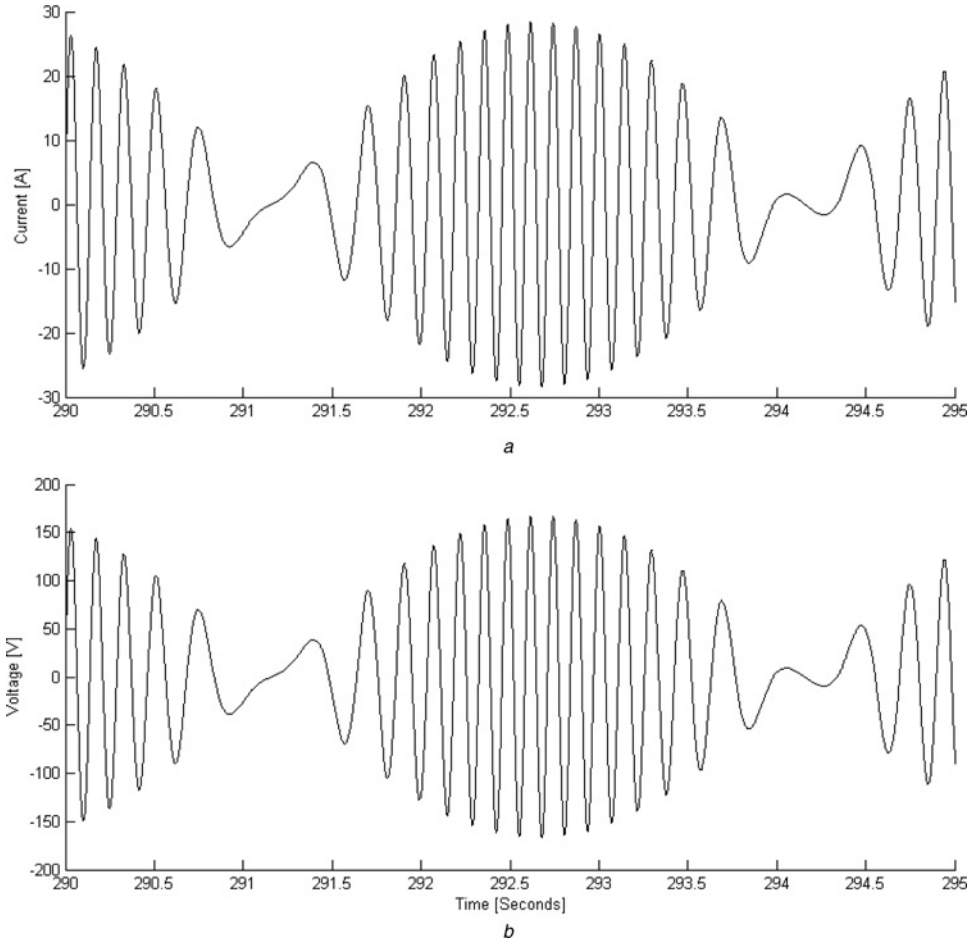

Fig. 5 *Simulated outputs from the generator model connected to the resistive load*

a One of the three-phase currents flowing through the resistive load
b One of the three-phase voltages over the resistive load

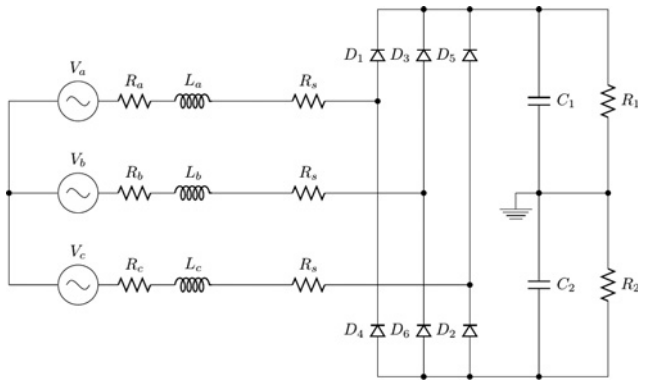

Fig. 6 *Circuit diagram of the passive rectification and the filter*

Table 3 Parameters for the passive rectification

C_1	C_2	R_1 (EXP)	R_2 (EXP)	R_1 (ADJ)	R_2 (ADJ)
24.52 F	24.52 F	6.84 Ω	6.84 Ω	6.66 Ω	6.66 Ω

which supplies the storage energy to the circuit. Large capacitance of the capacitors lowers the ripple factor [13] of both the converted DC voltage and DC current flowing through the load, and rises the amplitudes of the ripple voltage between the peaks of the load voltage. The ripple factor is calculated according to Equation (9), where $f = 2 \times$ *line frequency*. This simulation runs for nearly 300 s to get the load voltage output at the specific level observed in Fig. 7*b*. Nevertheless, the capacitor bank succeeded to upgrade the

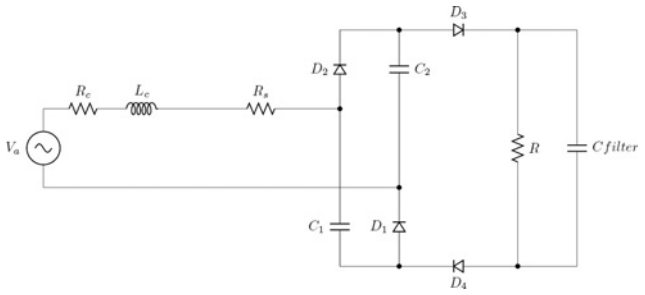

Fig. 8 *Circuit diagram of the resonant circuit in one phase*

power factor, as shown in Section 4.1

$$r = \frac{1}{2\sqrt{2}\pi^2 f^2} \cdot \frac{(C_1 + C_2) \cdot (R_1 + R_2)}{C_1 C_2 R_1 R_2} \tag{9}$$

3.2.3 Resonant rectification: The resonant circuit was previously developed by Boström [14] at Uppsala University and has been tested in the Lysekil research site. Fig. 8 shows one phase of the circuit diagram. The purpose of the circuit is to increase the damping factor and thus to extract more wave energy and deliver more power to the load compared with the passive rectification case. More details about the design and the theory of the circuit are provided in [15, 16]. The parameters of the circuit are presented in Table 4, which are also utilised for the simulation to observe the response from the generator model.

Fig. 9 presents the simulated result with the generator model. The rectifier circuit succeeds to achieve short-term energy storage while the AC voltage was rectified to the DC voltage.

The capacitor is discharging to stabilise the rectified voltage, while the diode's threshold voltage drops. It can be observed in Fig. 9*a*,

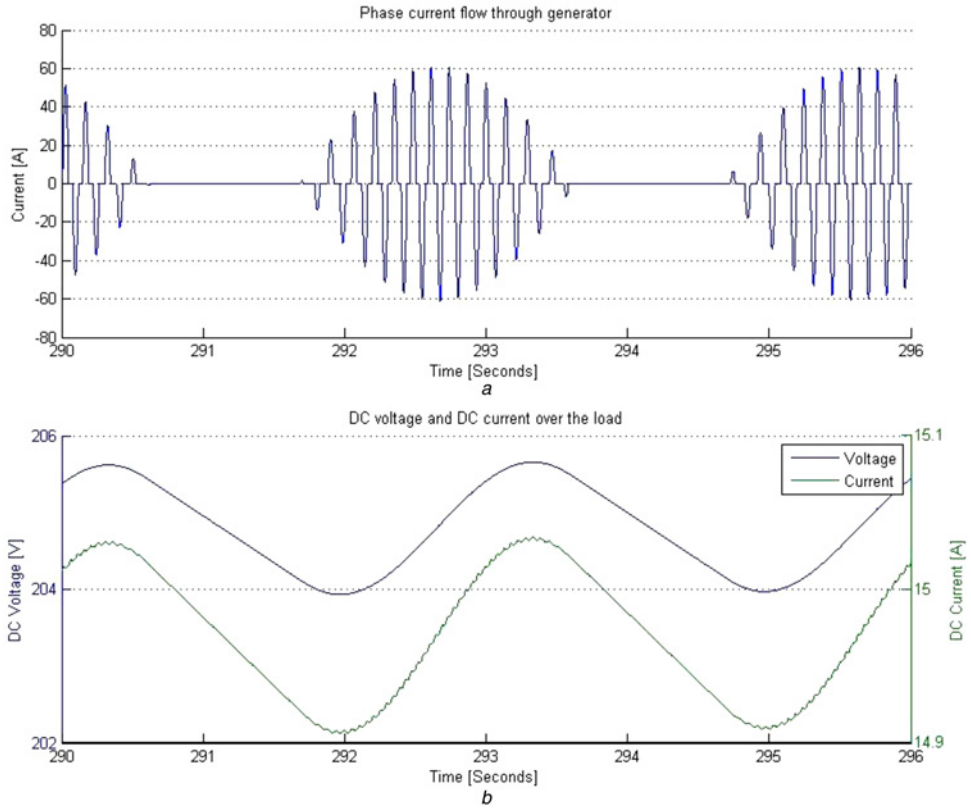

Fig. 7 *Simulated response of the generator connected to passive rectification and a capacitive filter*

a One of the three-phase currents flowing through the generator and rectifiers
b DC voltage over the resistive load on the rectified end and the load current

IET Renew. Power Gener., 2016, Vol. 10, Iss. 3, pp. 349–359

Table 4 Parameters for the resonant rectification

C_1	C_2	C_{filter}	R
0.017 F	0.017 F	0.009 F	5 Ω

comparing with the passive rectification case in Fig. 7*a*. Moreover, the electrical frequency is also to be considered. For the capacitor, it is not possible to prevent the small flow of the current with high frequency, whereas the current with low frequency easily gets through, if the voltage over the capacitor is close to DC voltage. Additionally, the polarity of the capacitor also leads to an increase of the whole amplitude. This will contribute to the ripples on the DC voltage as well, see Fig. 9*b*. Fig. 9*b* describes the DC output voltage over a resistive load as well as the load current. The ripples of the voltage are caused by the resonance between the capacitance and the resistance in the load system. Actually there is a capacitor connected in parallel with the DC load, which reduces the ripples of the overall load voltage, according to (10). However, the filter is not large enough for establishing a constant DC output

$$r = \frac{1}{2\sqrt{2}\pi^2 f^2} \cdot \frac{2C_{\text{filter}} + C'}{C' C_{\text{filter}} R_3}, \quad C' = C_1 \parallel C_2 \tag{10}$$

4 Results

Three different load circuits have been studied. The significance with the load cases is to observe how much energy can be captured with different strategies. For all the load cases, the same generator model has been used. The phase currents and load voltages agree well with experimental and theoretical results, see Fig. 3. To make an easier comparison between the different load strategies, the energy that the generator generates has been kept constant and equal for all loadings. Instead, to achieve the same generator energy within the same time period, necessary adjustments of the loads have been done. The total energy generated under 300 s by the generator was set to 282.5 kWh. The loads are adjusted according to the tables in Section 3.

4.1 Damping force

The passive rectification load case [(b) to represent] and resonant circuit load case [(c) to represent] both have capacitive components inside the circuit. These components introduce reactive power into the system. This resonant power leads to ripples with high frequency in the electrical damping force (see Figs. 10*b* and *c*) in the voltage and currents. According to (11), the damping force is calculated.

The damping force is calculated by

$$F_{\text{damp}} = \gamma(\dot{x}) A_{\text{fac}}(x) \dot{x}(t) \tag{11}$$

γ is the velocity-dependent damping function calculated by (12)

$$\begin{aligned} F_{\text{damp}} &= \gamma(\dot{x}) A_{\text{fac}}(x) \dot{x}(t)\ V_g\ V_{\text{load}}\gamma \\ &= 3\left[\frac{1}{R_g}\left(\frac{V_g}{\dot{x}}\right) + \frac{1}{R_c}\left(\frac{V_{\text{sea}}}{\dot{x}}\right) + \frac{3}{R_{\text{load}}}\left(\frac{V_{\text{load}}}{\dot{x}}\right)^2\right] \end{aligned} \tag{12}$$

where V_g, V_{sea}, and V_{load} are, respectively, the voltage drops over the resistances of the generator, the sea cable, and the load [7].

Nevertheless, the large capacitive filter is dramatically responsible for short-term energy storage and has the effect of increasing the system's power factor, as shown by the smaller ripples in Fig. 10*b*. The damping forces for three load cases have been compared under the same energy output from the linear generator (282.5 kWh). Within the same period, case (b) achieves a much higher magnitude of the damping force compared with the other cases.

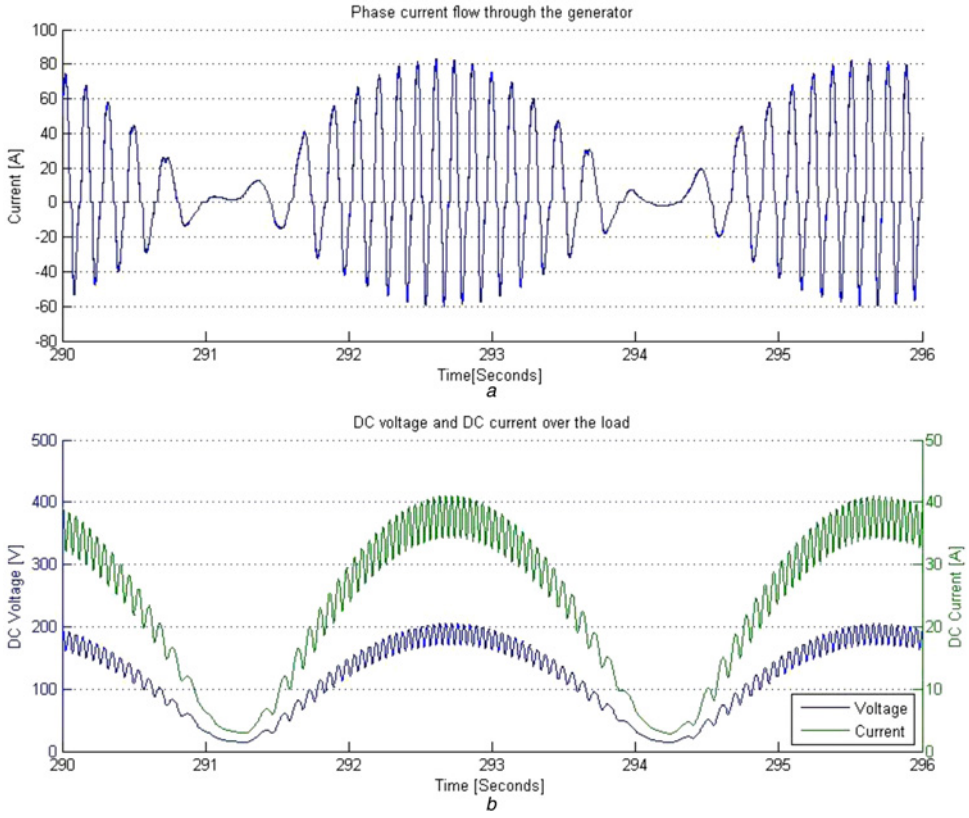

Fig. 9 *Simulated response of the generator connected to the resonant circuit*

a One of the three-phase currents through the generator and resonant circuit
b DC voltage over the resistive load and the load current

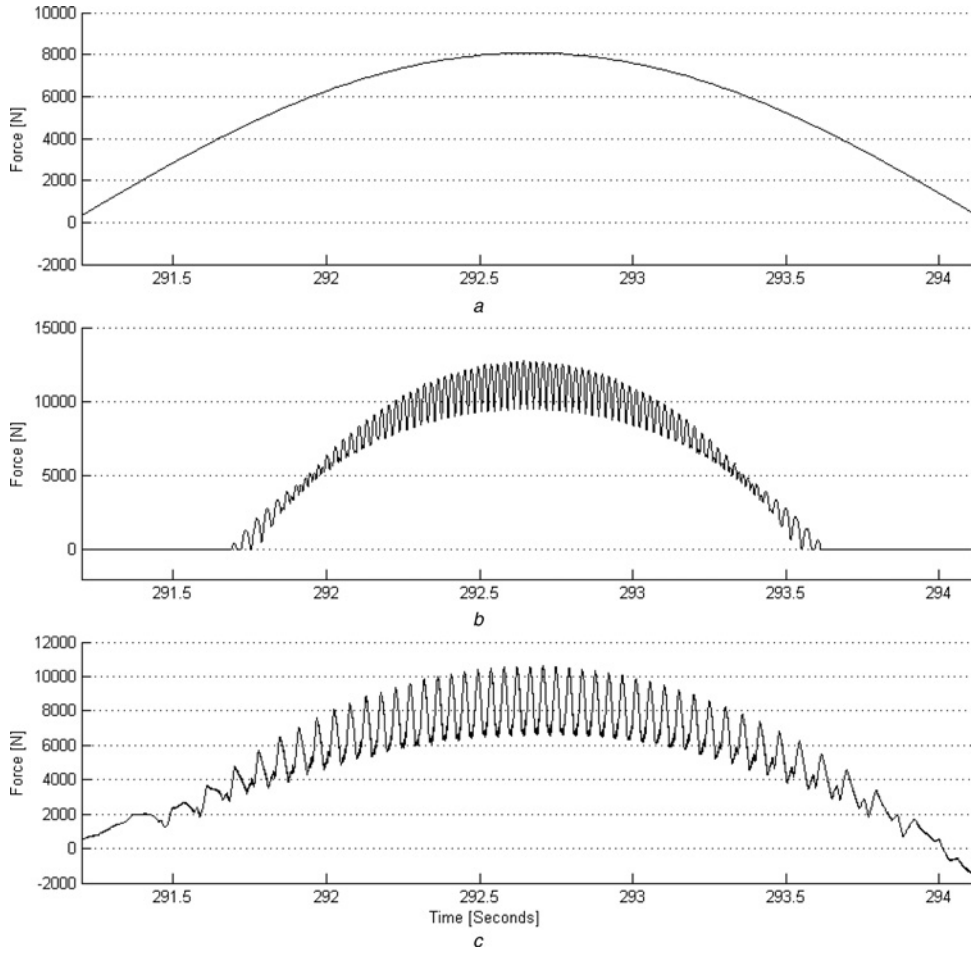

Fig. 10 *Electrical damping force with different load cases*

a Resistive load case
b Passive rectification case
c Resonant circuit case

The power factor on the linear generator is also studied. The results with three load cases are presented in Fig. 11. For case (a) the linear generator with resistive load is supposed to gain the highest power factor among the three cases; however, there also occurs small collapse possibly due to conditions when the translator's speed reduced to zero, this problem is observed at

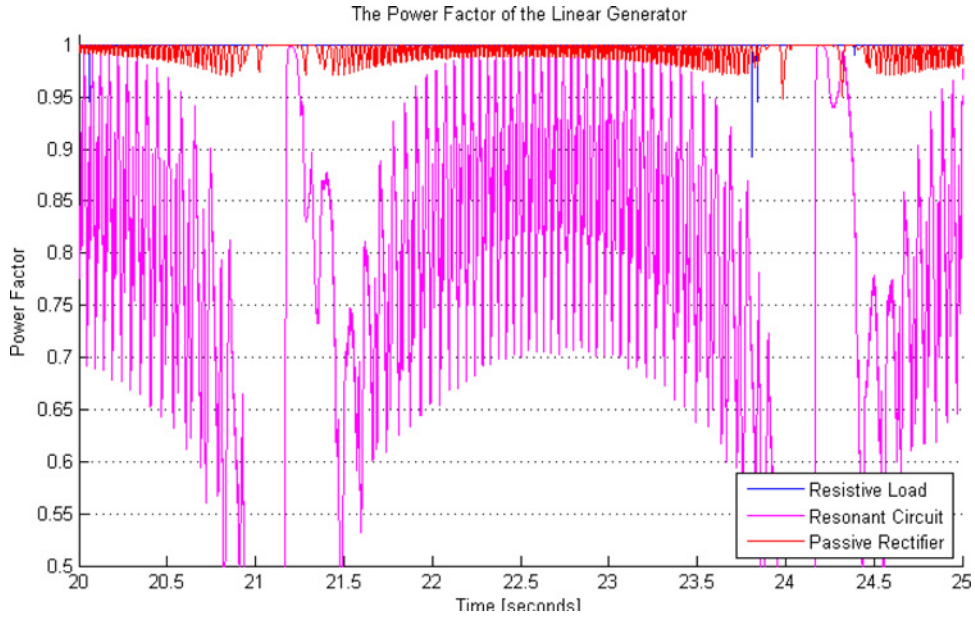

Fig. 11 *Power factor of the linear generator for the three load cases*

IET Renew. Power Gener., 2016, Vol. 10, Iss. 3, pp. 349–359

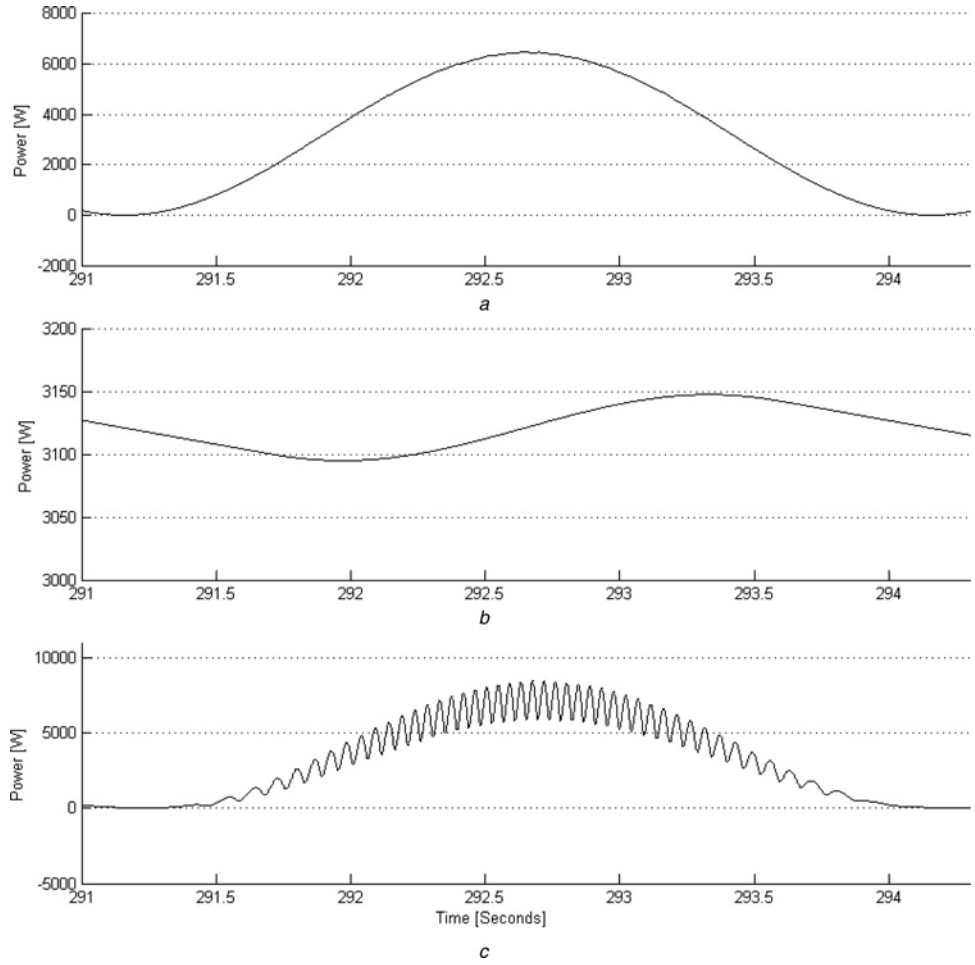

Fig. 12 *Simulated power production over the load with different load cases*

a Resistive load case
b Passive rectification case
c Resonant circuit case

23.8 s in Fig. 11. The power factor for case (b) varies between 0.95 and 1. It is thus not as high as case (a), but more stable than case (c) – a result of the very large capacitive filter on the load side.

4.2 Power in the load

The power at the load for the three different load cases is shown in Fig. 12.

In the linear load case shown in Fig. 12*a*, the power profile shows no resonant component and is in phase with the damping force. Owing to the large capacitance of the filter, the obtained DC voltage over the load is steady for case (b), as seen in Fig. 12*b*. The ripples over the profile, caused by the resonant effect (Fig. 12*c*), are more notable.

Since this paper is focused on the comparison among three different load cases, the comparison among different values for the same type load case is not made. However, related experiments have already been carried out and the comparison among different values for the same type load case was studied with the experimental results. More details are shown in [17, 18].

4.3 Energy losses

The accumulated energy loss as function of time for the three different load cases is shown in Fig. 13. The efficiency is calculated according to (13). The best efficiency for the studied case is obtained with a resistive load. The efficiency is about 90%. Most losses are seen in case (c), which has an efficiency of about 65%

$$\eta = \frac{P_{\text{load}}}{P_{\text{generator}}} \tag{13}$$

For the resistive load, the efficiency $\eta = P_{\text{load}}/P_{\text{generator}}$ is steady at about 90.8%; the steadiest among the three as there is little ripple occurring throughout the 300 s of simulation. The energy loss comes from the resistive losses in the generator and sea cables. The efficiency of the passive rectification case is more complex. It is affected by the charge level of the filter capacitors. When the efficiency attained a steady status, it reached 78%. The reason for the initial lower efficiency is that the large capacitor was charging on the load side. At steady state the main losses come from the passive rectifiers. Among the three, the resonant circuit gained the lowest energy efficiency, landing at 66%. For the resonant circuit, more diodes are used compared with the passive rectification load case, and this is the main reason for the lower efficiency. Furthermore, it is interesting to note that when the parameters of all the elements were set as the parameters in the experiments, then the passive rectification gains the highest energy efficiency and the resonant circuit the lowest.

5 Conclusions

A linear generator model, including the hydrodynamic driving forces and electrical loads, has been evaluated and shown to match the

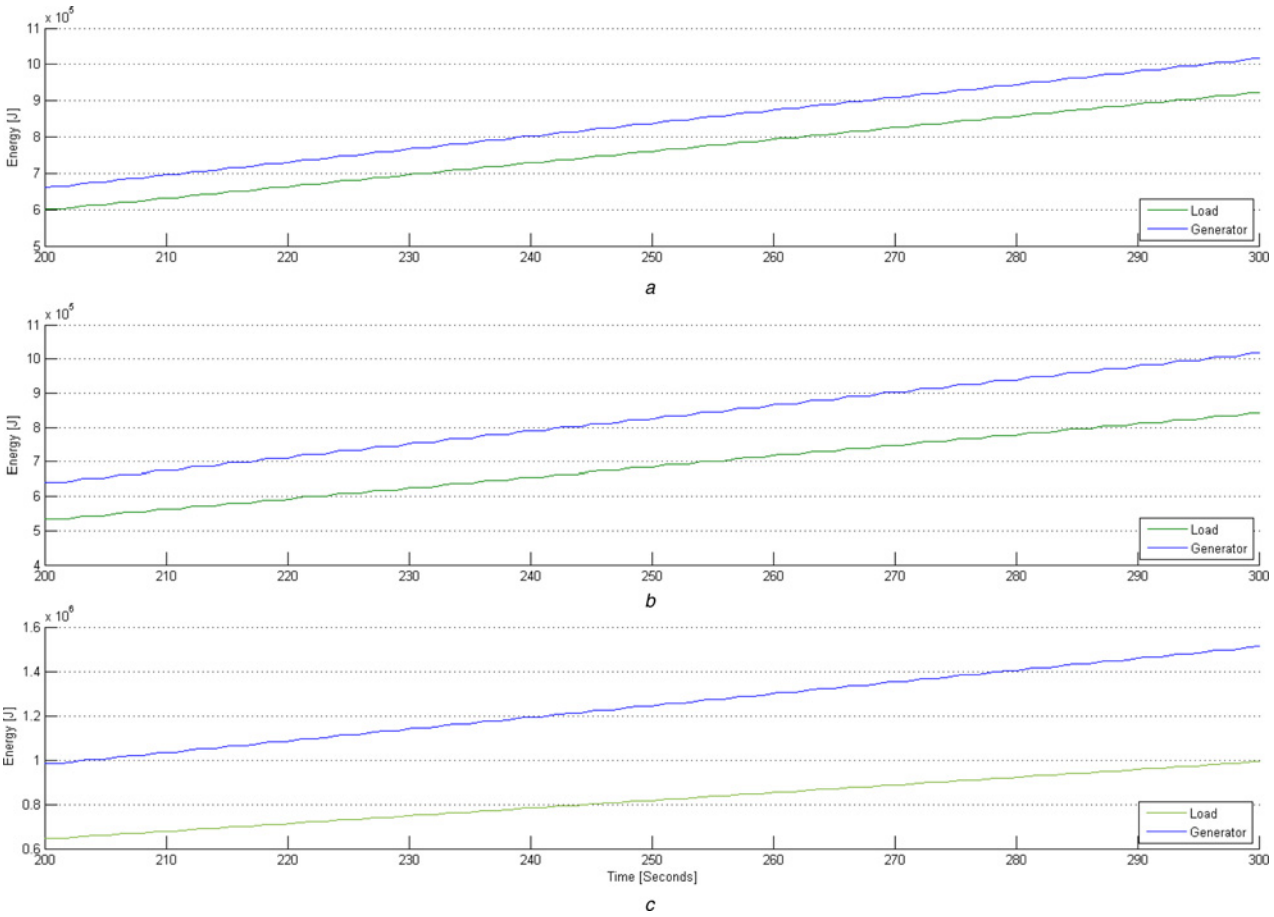

Fig. 13 *Comparison between extracted wave energy and the electrical energy production from 200 to 300 s during a 300 s simulation*

a Resistive load case
b Passive rectification case
c Resonant circuit case

experimental results of a prototype WEC in the Lysekil Project on the Swedish West coast. After validation, the generator model was run against three passive load strategies – linear resistive load, passive rectification, and resonance circuit. Owing to the non-linearity of the loads and speed of simulation only harmonic waves were studied – resulting in qualitative results on the nature of these passive strategies. For ease of comparison, the total energy has been kept constant throughout the study. The results give an indication of the efficiency of energy production as well as force ripples and resulting mechanical loads on the WECs. This is a well-known fact for wave power – the mechanical loads are important in a survival and maintenance perspective – which are just as important as the energy efficiency when considering the economy of a WEC.

The results show that under the studied test conditions the resistive load connection achieved the highest energy efficiency, 90.8%, among the three, whereas resonant rectification had the lowest energy efficiency, 66%. Resonant rectification also showed the highest peaks and largest ripples in power production, attributed to the higher damping forces achieved during this load strategy – this suggests that the cogging forces are the largest during this strategy which in turn increases the challenge of survivability and maintenance.

It is important to note that this is a limited study. Although the parameters for each strategy have been chosen to match large-scale experiments at the Lysekil research site and although the results give an indication of how these three strategies compare with each other, the study does not ultimately answer the question of which is the best passive strategy for harvesting ocean energy for the studied concept. Potential research questions for future studies would be to search for the optimum load parameters for each of the three passive strategies, and to vary the wave climate.

6 Acknowledgments

This work was supported by the SweGRIDS, Knowledge and Innovation Community, InnoEnergy-Controllable and Intelligent Power Components, Vetenskapsrådet, Statkraft Aksjeselskap (AS), Fortum Osakeyhtiö, the Swedish Energy Agency, Seabased Industry AB, Chinese Scholarship Council, Draka Cable Aktiebolag (AB), the Gothenburg Energy Research Foundation, Falkenberg Energy AB, Helukabel, Proenviro, ÅF Group, Vinnova, the Foundation for the Memory of J. Gust, Richert, the Göran Gustavsson Research Foundation, Vargöns Research Foundation, Swedish Research Council grant no. 621-2009-3417, and the Wallenius Foundation for their support of the project.

7 References

1 Waters, R., Stålberg, M., Danielsson, O., *et al.*: 'Experimental results from sea trials of an offshore wave energy system', *Appl. Phys. Lett.*, 2007, **90**, (3), p. 034105
2 Waters, R.: 'Energy from ocean waves: full scale experimental verification of a wave energy converter'. PhD thesis, Uppsala University, 2008
3 Hong, Y., Hultman, E., Castellucci, V., *et al.*: 'Status update of the wave energy research at Uppsala University'. Proc. 10th European Wave and Tidal Conf., Aalborg, Denmark, 2–5 September 2013
4 Ekström, R., Ekergård, B., Leijon, M.: 'Electrical damping of linear generators for wave energy converters – a review', *Renew. Sustain. Energy Rev.*, 2015, **42**, pp. 116–128

5 Krishna, R., Svensson, O., Rahm, M., *et al*.: 'Analysis of linear wave power generator model with real sea experimental results', *IET Renew. Power Gener.*, 2013, **7**, 5, pp. 574–581
6 Eriksson, M.: 'Modelling and experimental verification of direct drive wave energy conversion'. PhD thesis, Uppsala University, 2007
7 Eriksson, M., Waters, R., Svensson, O., *et al*.: 'Wave power absorption: experiments in open sea and simulation', *J. Appl. Phys.*, 2007, **102**, p. 084910
8 Waters, R., Rahm, M., Eriksson, M., *et al*.: 'Ocean wave energy absorption in response to wave frequency and amplitude – offshore experiments on a wave energy converter', *IET Renew. Power Gener.*, 2011, **5**, (6), pp. 465–469
9 Castellucci, V., Abrahamsson, J., Svensson, O., *et al*.: 'Algorithm for the calculation of the translator position in permanent magnet linear generators', *J. Renew. Sustain. Energy*, 2014, **6**, p. 063102
10 Eriksson, M., Isberg, J., Leijon, M.: 'Hydrodynamic modelling of a direct drive wave energy converter', *Int. J. Eng. Sci.*, 2005, **43**, (17–18), pp. 1377–1387
11 Eriksson, M., Isberg, J., Leijon, M.: 'Theory and experiment on an elastically moored cylindrical buoy', *IEEE J. Ocean. Eng.*, 2006, **31**, (4), pp. 959–963
12 Bostrom, C., Waters, R., Lejerskog, E., *et al*.: 'Study of a wave energy converter connected to a nonlinear load', *IEEE J. Ocean. Eng.*, 2009, **34**, (2), pp. 123–127
13 Malmstadt, H.V., Enke, C.G., Toren, E.C.: 'Electronics for scientists' (Physics Today, 1963)
14 Boström, C.: 'Electrical systems for wave energy conversion'. PhD thesis, Uppsala University, 2011
15 Ekergård, B., Boström, C., Hagnestål, A., *et al*.: 'Experimental results from a linear wave power generator connected to a resonance circuit', *WIREs Energy Environ.*, 2013, **2**, pp. 456–464
16 Boström, C., Ekergård, B., Waters, R., *et al*.: 'Linear generator connected to a resonance-rectifier circuit', *IEEE J. Ocean. Eng.*, 2013, **38**, (2), pp. 255–262
17 Boström, C., Leijon, M.: 'Operation analysis of a wave energy converter under different load conditions', *IET Renew. Power Gener.*, 2015, **3**, pp. 245–250
18 Boström, C., Lejerskog, E., Tyrberg, S., *et al*.: 'Experimental results from an offshore wave energy converter', *ASME. J. Offshore Mech. Arct. Eng*, 2010, **132**, (4), pp. 041103–041103-5